


**Anderson localization of surface plasmons in monolayer graphene**

Milad Sani and M. Hosseini Farzad\*

*Physics Department, College of Science, Shiraz University, Shiraz, Iran* (Received 21 November 2017; revised manuscript received 16 January 2018; published 6 February 2018)

Graphene is a two-dimensional material that has been highly regarded with its unique features to excite surface plasmonic waves. In this paper, we present the Anderson localization of surface plasmons in monolayer graphene. Here we proposed an active plasmonic device that consists of a monolayer graphene on silicon random grating to trap the surface plasmons in local cavities that are created by random multiple scattering. The quality factor of localized graphene surface plasmons (GSPs) is greater than the corresponding factor for uniformly distributed GSPs in periodic silicon substrate (reported before) up to three times. The field intensity of spatially localized GSPs in monolayer graphene is increased by a factor of 15 compared to GSPs in periodic grating. Our simulation results also show that the bandwidth of excitation spectrum of GSPs is extended as a result of introducing randomness in period in order to realize the desired random grating structure. Although the tuning of resonance frequencies of Anderson localized GSPs is a challenging task due to its random nature, here we tune the resonance frequencies of localized surface plasmons by using an external gate voltage for adjusting the Fermi level of monolayer graphene.

DOI: [10.1103/PhysRevB.97.085406](https://doi.org/10.1103/PhysRevB.97.085406)

Surface plasma waves are coherent oscillation of free electrons in metal which are coupled with an incident electromagnetic wave and play an important role in nanostructure devices. The emergence of very thin two dimensional materials like graphene improved the feature of plasmonic waves in these materials ranging from highly confined surface plasmons with relatively low loss to tunability of graphene carrier density or resonance frequency of graphene surface plasmons (GSPs); compare to traditional metals plasmonic materials [1–11]. Due to exotic properties of GSPs they can be used in many practical applications, such as biological sensing [12], plasmonic graphene ribbon waveguide [13], plasmonic modulators [14], detectors [15], and metamaterials [16].

Beside the interesting features of GSPs their excitations are in an acute contention in recent years, since there is a phase mismatch between incident wave vector of electromagnetic field in free space and GSP wave vector. Micro- and nanoribbon arrays as a substrate for monolayer graphene are more attracted to remove the phase matching problem by researchers [17–23]. In this approach there is no need to pattern graphene sheet, like in the micro- and nanoribbons graphene arrays method, and therefore the quality of carrier mobility is increased and improves the excitation efficiency of plasmonic waves in monolayer graphene.

On the other hand, study of Anderson localization (AL) of surface plasmonic waves has attracted extensive attention in recent years [24–27]. This localization for plasmonic waves is a consequence of interference effects that are created by multiple scattering of propagating waves in a disordered medium. Under this situation the diffusive transport of wave across the medium is converted to spatially localized plasmonic wave. Due to the subwavelength confinement of plasmonic waves in monolayer graphene, the multiple scattering effects are more pronounced

for GSPs. As a result of radiation leakage and inherent ohmic loss of plasmonic waves in traditional plasmonic materials the emergence of AL in these materials is a challenging task. Although plasmonic waves in graphene are far from these disadvantages, the Anderson localization of plasmonic waves are not reported in graphene based random nanostructures until now.

In this paper we simulated the emergence of AL in an active plasmonic device based on graphene. This plasmonic device is composed of single layer graphene that covers the surface of random silicon nanograting. New localized GSP resonance frequencies (with respect to GSP resonance frequencies appear in periodic nanograting) can be excited by moderate disordered nanograting substrate. These localized random GSP modes are confined deep subwavelength and their quality factors are enhanced, from 60 for periodic gratings to a maximum of 150 for random grating. Here, we demonstrate that the bandwidth of excitation spectrum of GSPs are extended in random grating. The result shows that the localized GSP mode frequencies can be tuned with small change in the chemical potential of graphene. This structure opens new windows to fabricate high efficiency active modulators, sensors, metamaterials, and random metasurfaces based on graphene. Also, the localized GSP modes with high intensities can be used to study the nonlinear effects near the graphene sheet.

A schematic of the designed diffractive grating is shown in Fig. 1. As observed in Fig. 1(a), the monolayer graphene is placed on a silicon grating substrate and the structure is enclosed by air. The parameters  $w_1$ ,  $w_2$ ,  $h$ , and  $p$  are the width of the silicon trench, width of the air trench, depth of the trench, and period of grating ( $p = w_1 + w_2$ ), respectively. This structure is easy to fabricate by patterning and etching shallow trench on silicon wafer. A normal-incidence EM wave is used to excite GSPs in monolayer graphene. The direction of the incoming electric field is perpendicular to  $z$  axis along which the structure is infinite, in order to excite plasmonic waves in graphene.

\*hosseinif@shirazu.ac.ir

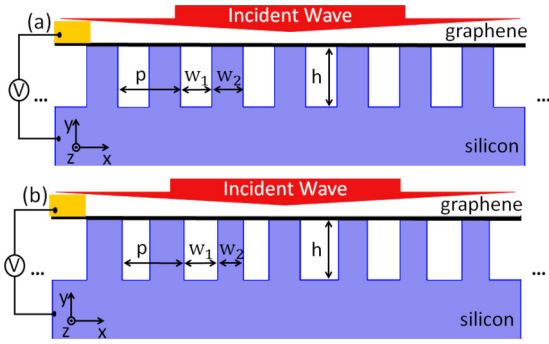


FIG. 1. Schematic illustration of the grating-graphene nanostructure under normal plane wave incidence. (a) Periodic grating (with zero randomness,  $\delta = 0\%$ ) with the following dimensions:  $h = 100$  nm,  $w_1 = w_2 = 50$  nm, and  $p = 100$  nm for the height, air trench, and silicon trench width of the grating and period, respectively. (b) Typical random grating with the same height of part (a) and random period with randomness strength of  $\delta = 20\%$ .

The thickness of the graphene layer is assumed to be 1 nm and the optical conductivity of graphene is calculated with random-phase approximation (RPA) as [28]

$$\begin{aligned} \sigma(\omega) = & \frac{2ie^2k_B T}{\pi\hbar^2(\omega + i\tau^{-1})} \ln \left[ 2 \cosh \left( \frac{E_f}{2k_B T} \right) \right] \\ & + \frac{e^2}{4\hbar} \left\{ \frac{1}{2} + \frac{1}{\pi} \arctan \left( \frac{\hbar\omega - 2E_f}{2k_B T} \right) \right. \\ & \left. - \frac{i}{2\pi} \ln \left[ \frac{(\hbar\omega + 2E_f)^2}{(\hbar\omega - 2E_f)^2 + (2k_B T)^2} \right] \right\}, \quad (1) \end{aligned}$$

where  $e$  is the electron charge,  $\omega/c$  is the wave vector of photon,  $k_B$  is the Boltzmann constant,  $T = 300$  K is the temperature,  $E_f = 0.62$  eV is the Fermi energy level, and  $\tau = \mu E_f / eV_f^2 = 6.2 \times 10^{-13}$  s is the momentum relaxation time, where  $V_f = 10^6$  m/s is the Fermi velocity and  $\mu = 10000$  cm<sup>2</sup>/(V s) is the carrier mobility of monolayer graphene. Anisotropic dielectric constant of monolayer graphene is described by a diagonal tensor where the out of plane graphene permittivity is  $\epsilon_{r11} = 2.5$  based on graphite dielectric constant and the in-plane graphene permittivity is characterized by dielectric function of  $\epsilon_{r22} = \epsilon_{r33} = 2.5 + i\sigma(\omega)/\epsilon_0\omega t$  in which  $\epsilon_0$  and  $t$  are vacuum permittivity and thickness of graphene layer, respectively. In our simulation, the spectrum range is below the optical phonon frequency of graphene ( $1667$  cm<sup>-1</sup>), so damping due to the electron interacting with the optical phonon is insignificant [29–31].

The multiple scattering of the incoming EM wave in this periodic grating can compensate the phase mismatch between EM wave vector and plasmonic wave vector. The phase match equation that relates the grating period ( $p$ ) and the incident EM frequency is given by  $\text{Re}[\beta(\omega_0)] = (\omega_0/c)\sin\theta + 2\pi/p$ , where  $c$  is the speed of light,  $\theta$  is the incident angle of the EM wave,  $\text{Re}[\beta(\omega_0)]$  is the real part of in plane plasmonic wave vector in graphene layer, and  $\omega_0/c$  is the vacuum wave vector  $k_0$ . The GSP modes would be excited at resonance frequencies that are evaluated from this phase match relation. As a result of coupling between guided mode resonance with incident EM wave, deep notches are created in the transmission spectrum. The cal-

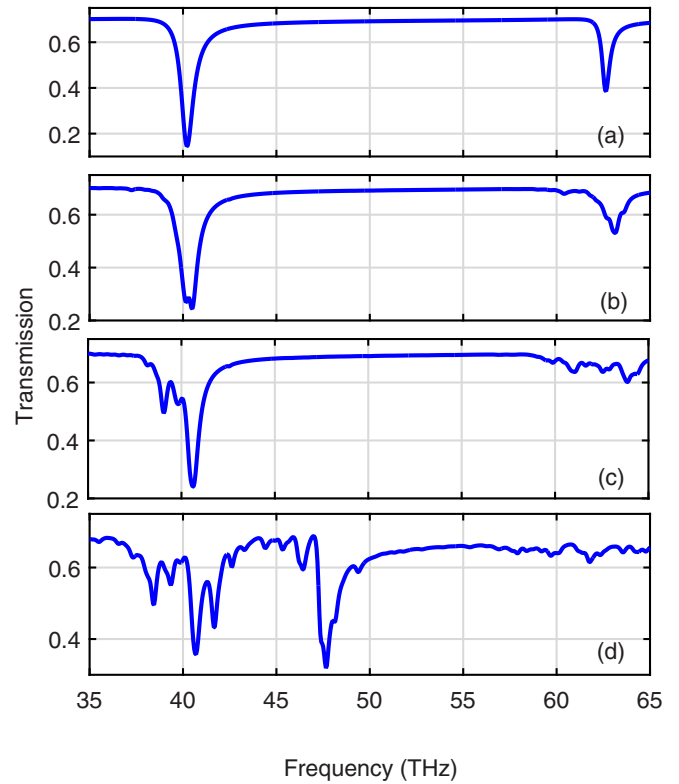


FIG. 2. Normal-incidence transmission spectrum of graphene based silicon grating for (a) periodic grating and random gratings with (b)  $\delta = 5\%$ , (c)  $\delta = 10\%$ , and (d)  $\delta = 20\%$ .

culated normal-incidence transmission spectrum for periodic grating is shown in Fig. 2(a). The deep notches in this figure are related to the excitation of first and second GSP resonance frequencies. According to Fig. 2(a), the first GSP normal mode at 38.7 THz has a  $Q$  factor of 60. The normalized field intensity distribution ( $|E_x|^2/|E_0|^2$ ) on the graphene layer as a function of frequency and the position on the graphene is shown in Fig. 3(a). Here  $|E_0|^2$  is the maximum value of  $|E_x|^2$  for periodic grating. Figure 3(a) illustrates that GSPs can be excited in narrow bandwidth around the first and second resonance frequencies in the periodic grating nanostructure. The sideview electric field distribution at first (38.7 THz) and second (54.8 THz) resonance frequencies for about  $2.5$   $\mu\text{m}$  of periodic grating in  $x$ - $y$  plane are shown in Figs. 4(a) and 4(b), respectively. Accordingly the number of lobes in one period is different in the spatial profile of the electric field (in  $x$ - $y$  plane) for these GSP modes.

The grating period is an important parameter to determine the resonance frequencies of GSP modes. Thus disorder is introduced in the period of diffractive grating by varying the width of air trench and silicon trench ( $w_1, w_2$ ) randomly by a fractional amount,  $\delta$ , along the grating. For example, a random grating with  $\delta = 10\%$  disorder means that the  $w_1$  and  $w_2$  width would be randomly changed between 45 nm and 55 nm for each silicon trench and air trench. Under this situation, the phase match relation is not satisfied because there is random value for period of grating and the GSP's resonance frequencies have been determined by random interference effect. Here we choose three levels of disorder,  $\delta$ , varying between 5% and 20% to study the influence of random diffractive grating in GSP

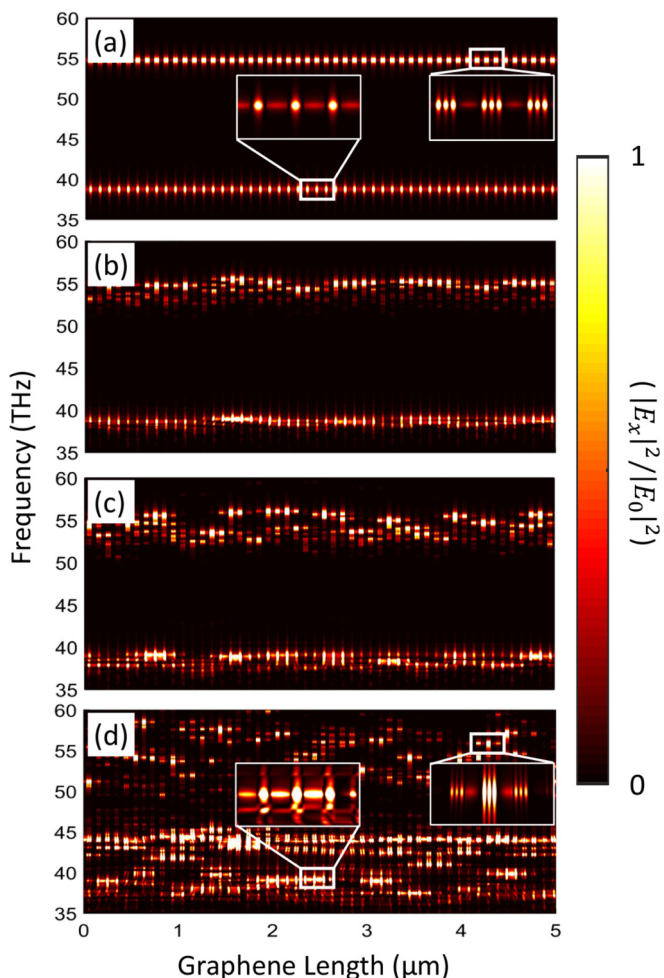


FIG. 3. Normalized field intensity distribution  $|E_x|^2/|E_0|^2$  as a function of frequency and the position on the graphene for (a) the periodic grating and for random gratings with (b)  $\delta = 5\%$ , (c)  $\delta = 10\%$ , and (d)  $\delta = 20\%$ . Here  $|E_0|^2$  is the maximum value of  $|E_x|^2$  for periodic grating.

modes. From the normal-incidence transmission spectrum for different randomness strength, see Figs. 2(b)–2(d), one can show the nonsmooth behavior of transmission around the above mentioned two modes (in periodic grating), so that many narrow notches (GSP resonance modes) are created around the resonance frequencies of the normal modes (in periodic case) that are shown in Fig. 2(d). By inspection of this figure it appears that the notch at 39.1 THz is nearly similar to the first mode of GSP in periodic structure and other resonance frequencies such as 37.4 THz and 44.1 THz are created by random interference effects. These additional random GSP modes show resonance with quality factors of 156 and 150, respectively. These highly localized GSP random modes with high quality factors reported here each show an evidence of Anderson localization of surface plasma waves in monolayer graphene. The high quality factor of GSP random modes indicates the lower rate of energy loss and higher stored energy in the spatially localized resonators which are deduced by Anderson localization effect.

The normalized field intensity ( $|E_x|^2/|E_0|^2$ ) distribution as a function of frequency and the position on the graphene

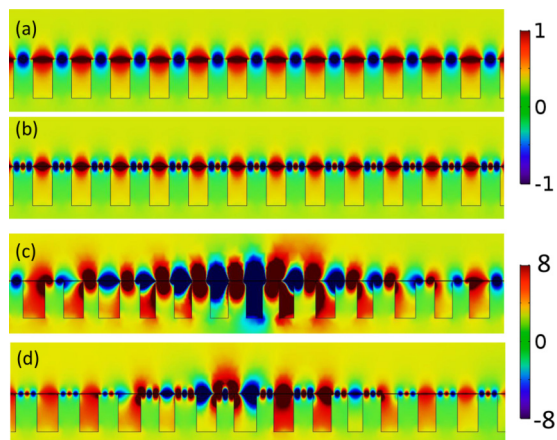


FIG. 4. Sideview  $E_x$ -field distribution for about 2.5  $\mu\text{m}$  along the graphene in  $x$ - $y$  plane for (a) first mode of periodic grating and (b) second mode of periodic grating. The  $E_x$ -field distribution for random mode at 37.4 THz and 44.1 THz in random grating with  $\delta = 20\%$  in (c) and (d), respectively.

for  $\delta = 5\%$  and  $\delta = 10\%$  is shown in Figs. 3(b) and 3(c), respectively. Here  $|E_0|^2$  is the maximum value of  $|E_x|^2$  for periodic grating. One can identify from these figures that the uniform distribution of  $E$ -field intensity for periodic grating [see Fig. 3(a)] has been disturbed by random interference effect and GSPs at a specific  $x$  position on graphene for frequencies inside the gap, dark region in part (a), are excited. Comparing the field distribution for random grating with  $\delta = 20\%$  [see Fig. 3(d)] with periodic grating [see Fig. 3(a)] reveals that the highly localized GSPs are excited in all frequencies except a small gap exists between 45 THz and 50 THz in random grating compared to a larger gap (between 38.7 THz and 54.8 THz) in periodic grating [Fig. 3(a)]. Therefore, the bandwidth of excitation spectrum of GSPs in random grating structure is broader than the corresponding bandwidth in the periodic grating.

The sideview electric field distribution for about 2.5  $\mu\text{m}$  of random grating in the  $x$ - $y$  plane at frequencies of 37.4 THz and 44.1 THz are plotted in Figs. 4(c) and 4(d), respectively. As observed in these figures, the field distribution is spatially localized in certain regions along the graphene which act like a resonator. The local resonators are created by random interference effects in random diffractive grating that caused the confined oscillations of carriers (spatially localized surface plasmon) in monolayer graphene which die out more slowly through the neighboring points in the  $x$  direction.

Figure 5(a) demonstrates the field intensity distribution as a function of frequency along the whole of the graphene layer for the first mode of periodic grating. As observed in this figure the GSPs are excited uniformly along the monolayer graphene. Figure 5(b) illustrates the same field intensity distribution for random grating with  $\delta = 20\%$ . By comparing the maximum intensity of GSPs in these two figures one can see that the amount of intensity in random grating is increased about 15 times the periodic one. This comparison manifests that the GSPs in graphene with periodic substrate are converted to highly localized GSPs in the random grating substrate due to Anderson localization effects. The extremely localized GSPs enhanced the EM intensity and consequently improved the

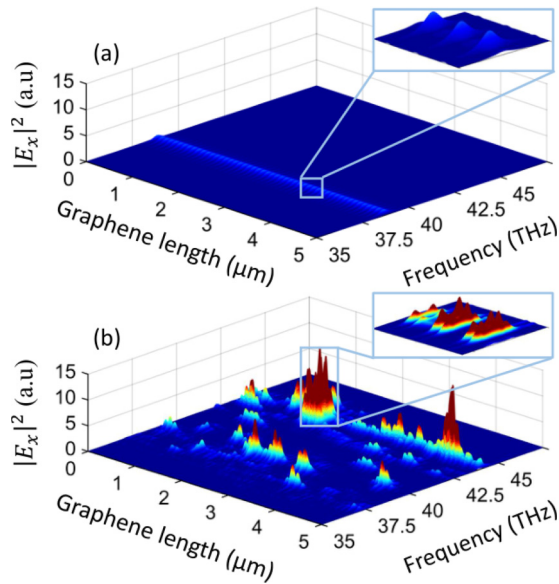


FIG. 5. Field intensity distributions as a function of frequency from 35 THz to 47.5 THz and the position on the graphene for (a) periodic grating [compare with Fig. 3(a)] and (b) random grating with  $\delta = 20\%$  [compare with Fig. 3(d)]. The subsets in parts (a) and (b) magnify a small portion of these 3D diagrams.

light-matter interaction over the monolayer graphene and it in turn proposed many new graphene plasmonic applications. Also, the localized GSP modes with high intensities can be used to study the nonlinear effects near the graphene sheet.

As we know the GSP resonance frequencies in an active periodic grating can be tuned fast by external adjusting of the Fermi level in graphene. On the other hand, frequency tuning of localized plasmonic waves in traditional plasmonic nanostructure (by metals) is a challenging task. Here, we demonstrate that a Fermi level change of 140 meV, by changing the gate voltage, causes a several THz shift of the localized GSP resonance frequencies appearing in transmission spectra of random grating with  $\delta = 20\%$ ; see the three curves in Fig. 6. According to this figure by increasing the value of Fermi

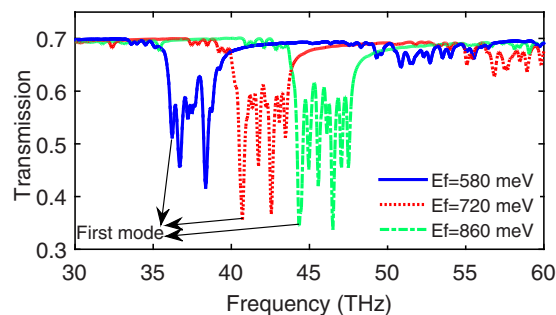


FIG. 6. Normal-incidence transmission spectra for different Fermi levels in structure with  $\delta = 20\%$ . The arrows show the first random mode equivalent to the first mode in periodic substrate; look at the first dip in Fig. 2(a).

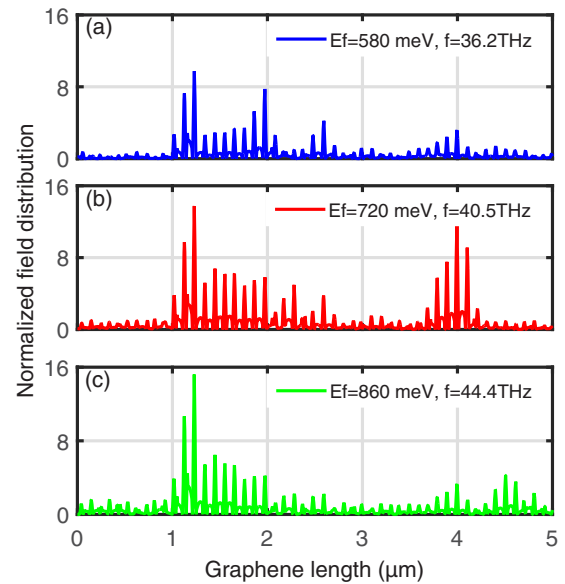


FIG. 7. Normalized field distribution ( $|E_x|^2/|E_0|^2$ ) along the whole of the graphene layer for (a) the first mode at 36.2 THz in transmission spectrum with  $E_f = 580$  meV, (b) the first mode at 40.5 THz in transmission spectrum with  $E_f = 720$  meV, and (c) the first mode at 44.4 THz in transmission spectrum with  $E_f = 860$  meV; see Fig. 6. Here  $|E_0|^2$  is the maximum value of  $|E_x|^2$  for periodic grating.

energy, the notches depth is increased since the excitation efficiency of GSP random modes is improved. The normalized field intensity distribution along the graphene layer for the first GSP modes in three transmission spectra represented in Fig. 6 are plotted in Fig. 7. It is shown from this figure that the spatial field distributions in these localized modes for different Fermi energy are nearly the same along the graphene layer. The general fact that is extracted from this figure is that only the type of the random grating substrate affects the general shape of the spatial field distribution of excited GSPs in monolayer graphene.

To conclude, we proposed a 2D active random plasmonic device to excite the surface plasmons in a broad bandwidth in monolayer graphene. The simulation results show that there is a transition from uniform intensity distributed GSP modes along the graphene in the periodic substrate excitation method to strongly localized GSP modes in the random substrate excitation method. These GSP modes occurred in several different frequencies more than the corresponding ones in a former method. We have shown that the resonance frequencies of strong localized GSPs can be tuned by adjusting the Fermi level in monolayer graphene. Furthermore, the spatially localized GSPs also have larger quality factor and field intensity compared to GSPs in periodic structure. The presented results will open a window to development of optoelectronic devices. Also, they may facilitate the preparation of next-generation optical integrated systems based on graphene nanostructures such as graphene based solar cell (increasing the solar absorption bandwidth), spatial light modulators, and plasmonic sensors.



- [1] J. D. Cox, R. Yu, and F. J. García de Abajo, *Phys. Rev. B* **96**, 045442 (2017).
- [2] A. N. Grigorenko, M. Polini, and K. S. Novoselov, *Nat. Photon.* **6**, 749 (2012).
- [3] F. H. L. Koppens, D. E. Chang, and F. J. García de Abajo, *Nano Lett.* **11**, 3370 (2011).
- [4] D. Jin, T. Christensen, M. Soljačić, N. X. Fang, L. Lu, and X. Zhang, *Phys. Rev. Lett.* **118**, 245301 (2017).
- [5] V. W. Brar, M. S. Jang, M. Sherrott, J. J. Lopez, and H. A. Atwater, *Nano Lett.* **13**, 2541 (2013).
- [6] D. A. Smirnova, A. E. Miroshnichenko, Y. S. Kivshar, and A. B. Khanikaev, *Phys. Rev. B* **92**, 161406 (2015).
- [7] J. Chen *et al.*, *Nature (London)* **487**, 77 (2012).
- [8] M. Farhat, S. Guenneau, and H. Bağcı, *Phys. Rev. Lett.* **111**, 237404 (2013).
- [9] P. Y. Chen, M. Farhat, A. N. Askarpour, M. Tymchenko, and A. Alù, *J. Opt.* **16**, 094008 (2014).
- [10] J. Schiefele, J. Pedrós, F. Sols, F. Calle, and F. Guinea, *Phys. Rev. Lett.* **111**, 237405 (2013).
- [11] R. Yu, V. Pruneri, and F. J. García de Abajo, *ACS Photon.* **2**, 550 (2015).
- [12] D. Rodrigo, O. Limaj, D. Janner, D. Etezadi, F. J. García de Abajo, V. Pruneri, and H. Altug, *Science* **349**, 165 (2015).
- [13] A. Yu. Nikitin, F. Guinea, F. J. García-Vidal, and L. Martín-Moreno, *Phys. Rev. B* **84**, 161407 (2011).
- [14] B. D. Thackray, P. A. Thomas, G. H. Auton, F. J. Rodriguez, O. P. Marshall, V. G. Kravets, and A. N. Grigorenko, *Nano Lett.* **15**, 3519 (2015).
- [15] D. B. Farmer, P. Avouris, Y. Li, T. F. Heinz, and S.-J. Han, *ACS Photon.* **3**, 553 (2016).
- [16] L. Ju *et al.*, *Nat. Nanotechnol.* **6**, 630 (2011).
- [17] N. Matthaikakakis, H. Mizuta, and M. D. B. Charlton, *Sci. Rep.* **6**, 27550 (2016).
- [18] F. Karimi and I. Knezevic, *Phys. Rev. B* **96**, 125417 (2017).
- [19] B. Zhao and Z. M. Zhang, *ACS Photon.* **2**, 1611 (2015).
- [20] J. Wang, H. Shao, C. Song, G. Zheng, Z.-D. Hu, and T. Sang, *AIP Adv.* **7**, 055204 (2017).
- [21] W. Gao, J. Shu, C. Qiu, and Q. Xu, *ACS Nano* **6**, 7806 (2012).
- [22] D. Rodrigo, T. Low, D. B. Farmer, H. Altug, and P. Avouris, *Phys. Rev. B* **93**, 125407 (2016).
- [23] J. Christensen, A. Manjavacas, S. Thongrattanasiri, F. H. L. Koppens, and F. J. García de Abajo, *ACS Nano* **6**, 431 (2012).
- [24] F. Rütting, *Phys. Rev. B* **83**, 115447 (2011).
- [25] F. Rütting, P. A. Huidobro, and F. J. García-Vidal, *Opt. Lett.* **36**, 4341 (2011).
- [26] J. A. Sánchez-Gil, *Phys. Rev. B* **68**, 113410 (2003).
- [27] W. Wang, S. Xiao, and N. A. Mortensen, *Phys. Rev. B* **93**, 165407 (2016).
- [28] L. A. Falkovsky and S. S. Pershoguba, *Phys. Rev. B* **76**, 153410 (2007).
- [29] M. Jablan, H. Buljan, and M. Soljačić, *Phys. Rev. B* **80**, 245435 (2009).
- [30] J. Tao, X. Yu, B. Hu, A. Dubrovkin, and Q. J. Wang, *Opt. Lett.* **39**, 271 (2014).
- [31] H. Yan, T. Low, W. Zhu, Y. Wu, M. Freitag, X. Li, F. Guinea, P. Avouris, and F. Xia, *Nat. Photon.* **7**, 394 (2013).